Computers and Structures 191 (2017) 115–128

Contents lists available at ScienceDirect

Computers and Structures

journal homepage: www.elsevier.com/locate/compstruc

Stress based topology optimization of reinforcement structure under in-plane load

Jong Wook Lee [a], Gil Ho Yoon [b,*]

[a] Graduate School of Mechanical Engineering, Hanyang University, Republic of Korea
[b] School of Mechanical Engineering, Hanyang University, Republic of Korea

ARTICLE INFO

Article history:
Received 20 October 2016
Accepted 25 May 2017
Available online 27 June 2017

Keywords:
Topology optimization
Stress constraints
Reinforcement
Singularity issue
Stress interpolation
Local optimum

ABSTRACT

As the static safety of mechanical structure is one of important criteria in engineering design process, it has been one of important topics to consider the static failure of a structure in topology optimization (TO). With the help of some recent relevant researches, some difficult issues in considering static failure are solved. However, this research found that the singularity issue which refers the difficulty of obtaining global optima with the KKT condition is not serious and mathematically relaxed for reinforcement TO design. And it is found that the existing qp-relaxation stress interpolation scheme to resolve the singularity issue in TO just shows the local optima issue in reinforcement TO design with different penalization factors in Solid Isotropic Material with Penalization (SIMP). In order to explain this feature, the TO problems for simple benchmark truss structures are revisited. Several two-dimensional examples only with in-plane load are solved to confirm the validity of the present study.

1. Introduction

This research considers the reinforcement design by topology optimization (TO) considering the stress failure constraint. After the development of TO, it has been widely applied for various engineering applications from microstructures to megastructures and from single physics system to multi-physics systems [1–10]. However, the stress based topology optimization problem (STOM) minimizing volume subject to local stress constraints has been considered as one of the most difficult problems due to the singularity issue, the many constraint issue and the highly nonlinear constraint issue. With the help of many important contributions, nowadays, it is possible to consider these stress constraints in TO and the stress constraints in multi-physics system. However, STOM is still regarded as one of important engineering problems and it should be extended to consider fatigue constraint [4,11–37]. One may think that this STOM also can be applied to the reinforcement design which finds out an optimal reinforcement design to constrain the maximum stress value. But applying STOM for the reinforcement design is not clear about the three issues: the singularity issue, the many constraint issue and the highly nonlinear constraint issue Particularly we found that the singularity issue needs an in-depth study and the role of the existing qp-relaxation method devised by many important relevant researches for the STOM also needs an in-depth investigation whether that method is valid or not for the STOM designing reinforcement structures [11,12,14,16,17,24,30,31,36–41].

The reinforcement structure increasing structural safety by adding some materials (reinforcements) to basic structures is common in civil and mechanical designs [42,43]. One merit of the usage of the reinforcement structure may be the non-destruction of basic structure and the increase of the safety. However, the reinforcement requires some extra materials and costs and the improper choice of the reinforcement structure can cause extra damages to basic structures. For examples, steel rib walls in ship building also can be regarded as reinforcements too (see Fig. 1).

To conduct the STOM minimizing volume subject to local stress constraints, it is very important to use the *qp*-relaxation method for the singularity issue with the *P*-norm approach for the local behavior of the stress constraints. The *qp*-relaxation method adopts the different penalization factors for the Young's modulus in the forward analysis and in the stress evaluation analysis; we do not have to limit to the penalization factors of the SIMP polynomial functions. Without this *qp*-relaxation method, the nominal stress values are decreased with smaller design values and what a gradient based optimizer face for TO with void and solid domains is that no-structure becomes a global optimum. In case of the reinforcement design, we found that this argument becomes unclear

* Corresponding author at: School of Mechanical Engineering, Hanyang University, Seoul, Republic of Korea.
E-mail addresses: ghy@hanyang.ac.kr, gilho.yoon@gmail.com (G.H. Yoon).

http://dx.doi.org/10.1016/j.compstruc.2017.05.009
0045-7949/

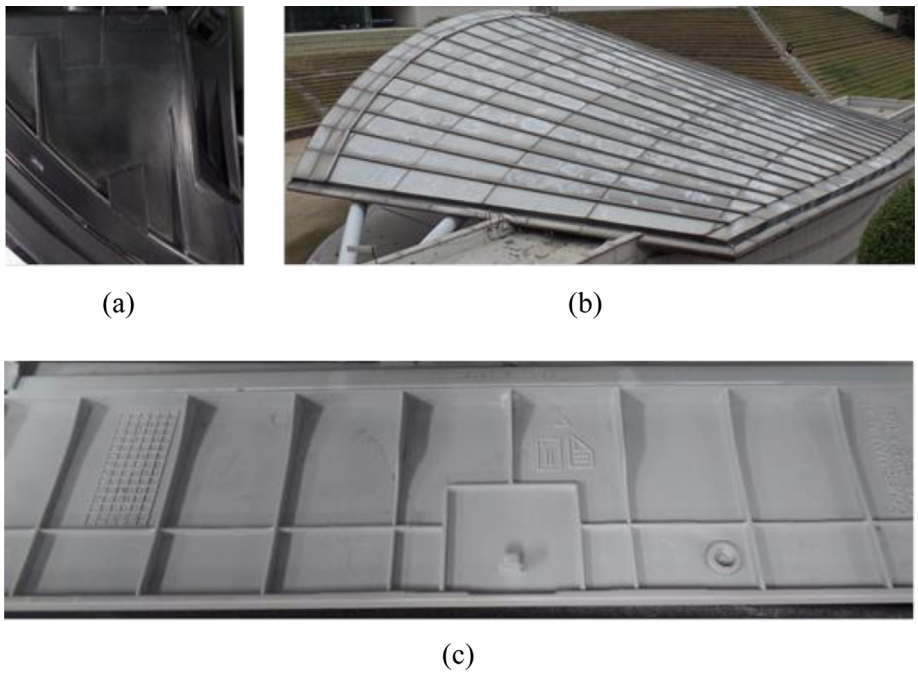

Fig. 1. Reinforcement structures in some architectures and machines: (a) rib structure in the automotive bonnet, (b) rib structure attached to roof and (c) plastic rib structures used in electronic device.

and obscure because of the existing of the basic (or base) structure in Fig. 1. To our best knowledge, the stress behaviors of reinforcement structures are not rigorously studied in TO. To address this unclear point, this research reinvestigates the singularity issue and the idea of the *qp*-relaxation method. In the present study, the in-plane load is only considered but the conclusions and findings can be applied for reinforcement structure with a combination of different types of loads.

The paper is organized as follows: In Section 2 and Section 3, the finite element formulation for reinforcement design is presented. The new singularity issue of reinforcement design with the existing *qp*-relaxation method is studied and some examples will be presented. Section 4 will provide several optimization examples to show the validity and effectiveness of the present stress interpolation issue. Finally, our findings are summarized in the conclusion.

2. Reinforcement design with finite element method and non-singularity issue

2.1. 2-dimensional finite element model with in-plane load

This section introduces a brief FE analysis for the reinforcement structure design considering the local stress constraints. To consider it in the FE framework, the following static finite element equations are employed [44]. Note that the thicknesses of reinforced structures can be increased and the central plane of rib may not be coplanar with the central plane of the original structure, *i.e.*, Fig. 1(c). Then the plane stress distribution in the rib along thickness direction may not be uniform even with in-plane load. The non-uniform stress distributions due to this side effect should be considered and this issue becomes critical in topology optimization when the stress distributions along thickness direction are not negligible for layerwise structure or functionally graded material (FGM) characterized by the variation in composition and structure gradually over volume.

$$\mathbf{KU} = \mathbf{F} \tag{1}$$

$$\mathbf{K} = \mathbf{K}_{\mathrm{R}} + \mathbf{K}_{\mathrm{B}} = \sum_{e=1}^{NE} (\mathbf{k}_{\mathrm{R},e} + \mathbf{k}_{\mathrm{B},e}) \tag{2}$$

$$\mathbf{k}_{\mathrm{R},e} = \iiint_V \mathbf{B}^{\mathrm{T}} \mathbf{C}_{\mathrm{R},e} \mathbf{B} dV, \mathbf{k}_{\mathrm{B},e} = \iiint_V \mathbf{B}^{\mathrm{T}} \mathbf{C}_{\mathrm{B},e} \mathbf{B} dV \tag{3}$$

$$\mathbf{C}_{\mathrm{R},e} = \gamma_e^n \mathbf{C}_0, \mathbf{C}_{\mathrm{B},e} = \mathbf{C}_0 \tag{4}$$

$$\text{Plane stress}: \quad \mathbf{C}_0 = \frac{E_0}{1-\nu^2} \begin{bmatrix} 1 & \nu & 0 \\ \nu & 1 & 0 \\ 0 & 0 & \frac{1-\nu}{2} \end{bmatrix} \tag{5}$$

where the global stiffness, the global displacement, and the global force vector are denoted by **K**, **U** and **F**, respectively. The global stiffness matrix is further decomposed into the two terms, $\mathbf{K}_{\mathrm{R}}$ for the reinforcement structure and $\mathbf{K}_{\mathrm{B}}$ for the basic structure as shown in Fig. 2. The *e*-th elementary stiffness matrices for the reinforcement structure and the basic structure are $\mathbf{k}_{\mathrm{R},e}$ and $\mathbf{k}_{\mathrm{B},e}$, respectively. The design variable, γ_e, is assigned with the SIMP (Solid Isotropic Material with Penalization) penalization, *n* to interpolate the constitutive matrix, $\mathbf{C}_{\mathrm{R},e} = \gamma_e^n \mathbf{C}_0$, for $\mathbf{k}_{\mathrm{R},e}$.

2.2. Non-singularity problem of the reinforcement in simple truss design problem

From our best knowledge, there is no precedent research about the singularity issue in reinforcement design. Therefore, this subsection investigates the singularity issue in the truss reinforcement design. The singularity issue in the stress based TO refers the difficulties in numerically finding the global optimum with the KKT condition [12]. To resolve this difficulty, many researches have been conducted [4,11–25,27–37].

With basic structure and reinforcement structure, each structure can have different stress interpolation functions, i.e., here the different penalization factors of the SIMP based interpolation function. In other words, the stresses are evaluated by (6).

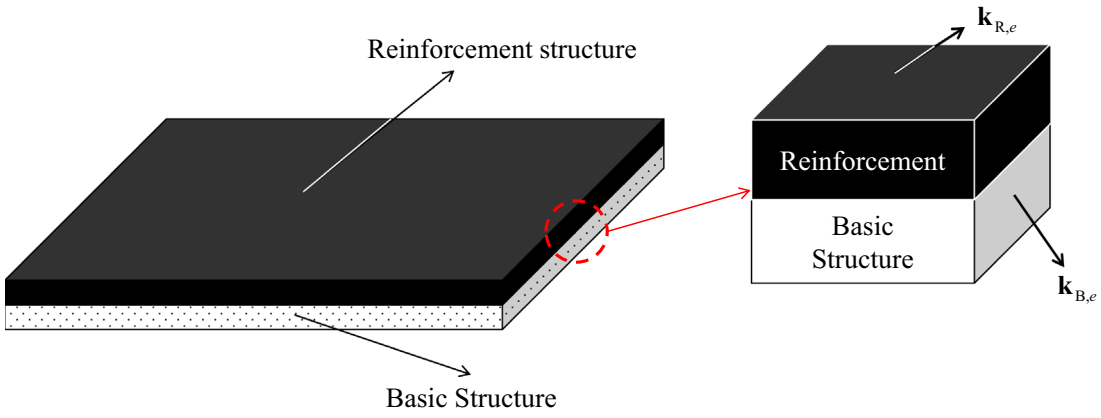

Fig. 2. The concept of the basic structure and the reinforcement structure with in-plane load.

$$\boldsymbol{\sigma}_{B,e} = \mathbf{C}_0\boldsymbol{\varepsilon}_e \tag{6.1}$$

$$\boldsymbol{\sigma}_{R,e} = \gamma^{n_s}\mathbf{C}_0\boldsymbol{\varepsilon}_e \tag{6.2}$$

The stresses of the e-th element of the reinforcement and the basic structure are denoted by $\boldsymbol{\sigma}_{B,e}$ and $\boldsymbol{\sigma}_{R,e}$, respectively. No to mention, the strains of the two structures are equal to $\boldsymbol{\varepsilon}_e$. The penalty factor, n_s, was set to 0.5 for the singularity issue in the relevant researches [21,24,26].

In the present study, we find out that the singularity issue is not serious for the reinforcement design. In here, it doesn't mean that there are no singular topologies. The meaning of "serious" is that an alternative material interpolation function can be adopted with 0.5 or 3 for ns to overcome the singular topologies. To illustrate this, first of all let us consider the simple truss structure in Fig. 3 with two elastic trusses. In this 1-D example, the two springs (or trusses) and the displacement at the right side is set to u.

With this configuration, the mechanical stress values at the two structures are computed as follows:

Forward analysis:

$$\varepsilon = \frac{u}{L} \tag{7.1}$$

$$E_R = E_{R_0}\gamma_R^{n_s}, \quad E_B = E_{B_0} \tag{7.2}$$

$$k_R = \gamma_R^n E_{R_0}k_0, \quad k_B = E_{B_0}k_0, \quad k_0 = \frac{A}{L}(\text{Hook's law}: \ (k_R + k_B)u = P) \tag{7.3}$$

$$\text{The stress at the basic structure}: \sigma_B = \frac{PE_B}{L(k_R + k_B)} = \frac{P}{Lk_0}\frac{E_{B_0}}{(\gamma_R^n E_{R_0} + E_{B_0})} \tag{8.1}$$

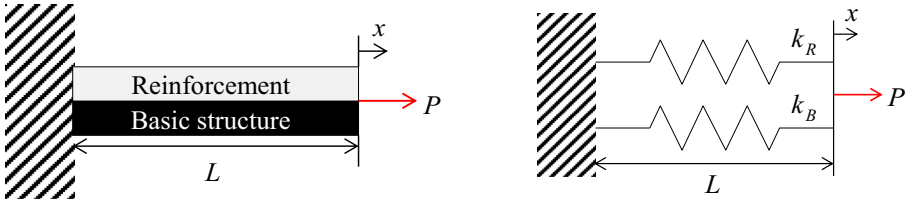

Fig. 3. Truss structure of the reinforcement and the basic structure.

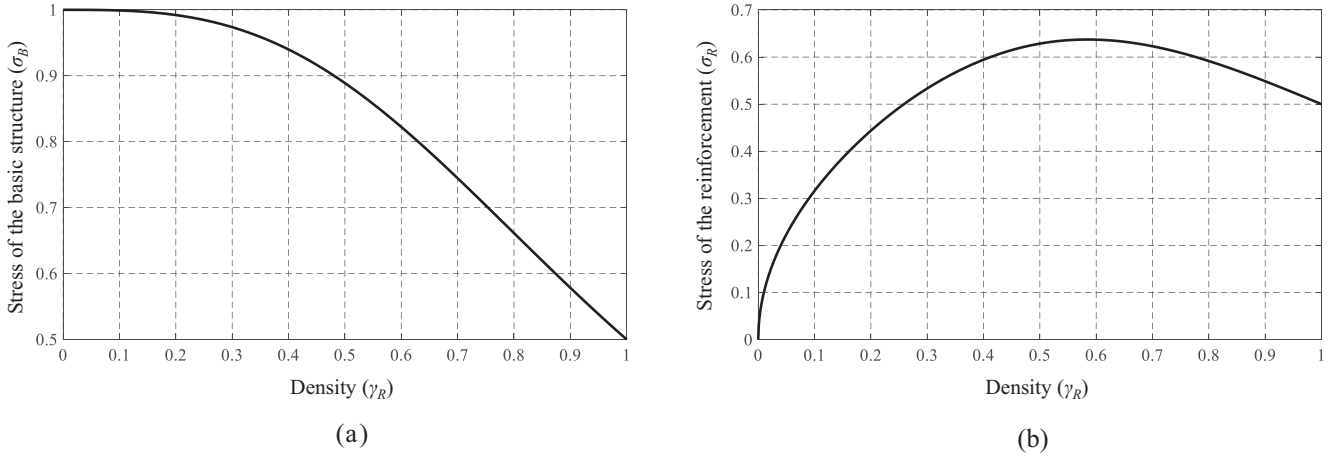

Fig. 4. Stress curves with the respect to the density variable (P = 1 N, E_{R0} = 1 Pa, E_{B0} = 1 Pa, L = 1 m, k_0 = 1 N/m, n = 3, n_s = 0.5): (a) the stress σ_B at the basic structure and (b) the stress σ_R at the reinforcement structure with qp-relaxation method (n_s = 0.5).

The stress at the reinforcement : $\sigma_R = \dfrac{PE_R}{L(k_R + k_B)}$

$$= \frac{P}{Lk_0}\frac{\gamma_R^{n_s} E_{R_0}}{(\gamma_R^n E_{R_0} + E_{B_0})} \tag{8.2}$$

$$\frac{\sigma_R}{\sigma_B} = \frac{\gamma_R^{n_s} E_{R_0}}{E_{B_0}} \tag{8.3}$$

where the length of the structure, the displacement, the strain, Young's modulus of the basic structure, Young's modulus of the reinforcement and the force are represented as L, u, ε, E_{B0}, E_{R0} and P, respectively. The above equations of (7) are for the forward analysis for the displacement and the equations of (8) are for the stress ratio of the two layers. The stiffness values of the basic structure and the reinforcement structure are k_B and k_R, respectively. Note that due to the singularity issue in the STOM, the qp-relaxation

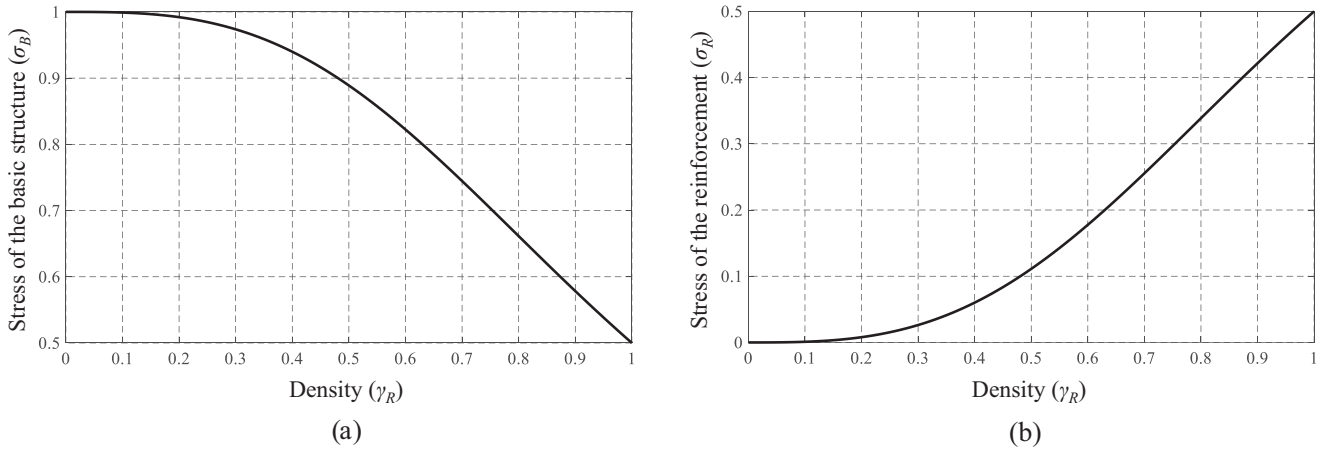

Fig. 5. Stress curves with the respect to the density variable (P = 1 N, E_{R0} = 1 Pa, E_{B0} = 1 Pa, L = 1 m, k_0 = 1 N/m, n = 3, n_s = 3): (a) the stress σ_B at the basic structure and (b) the stress σ_R at the reinforcement structure with qp-relaxation method (n_s = 3).

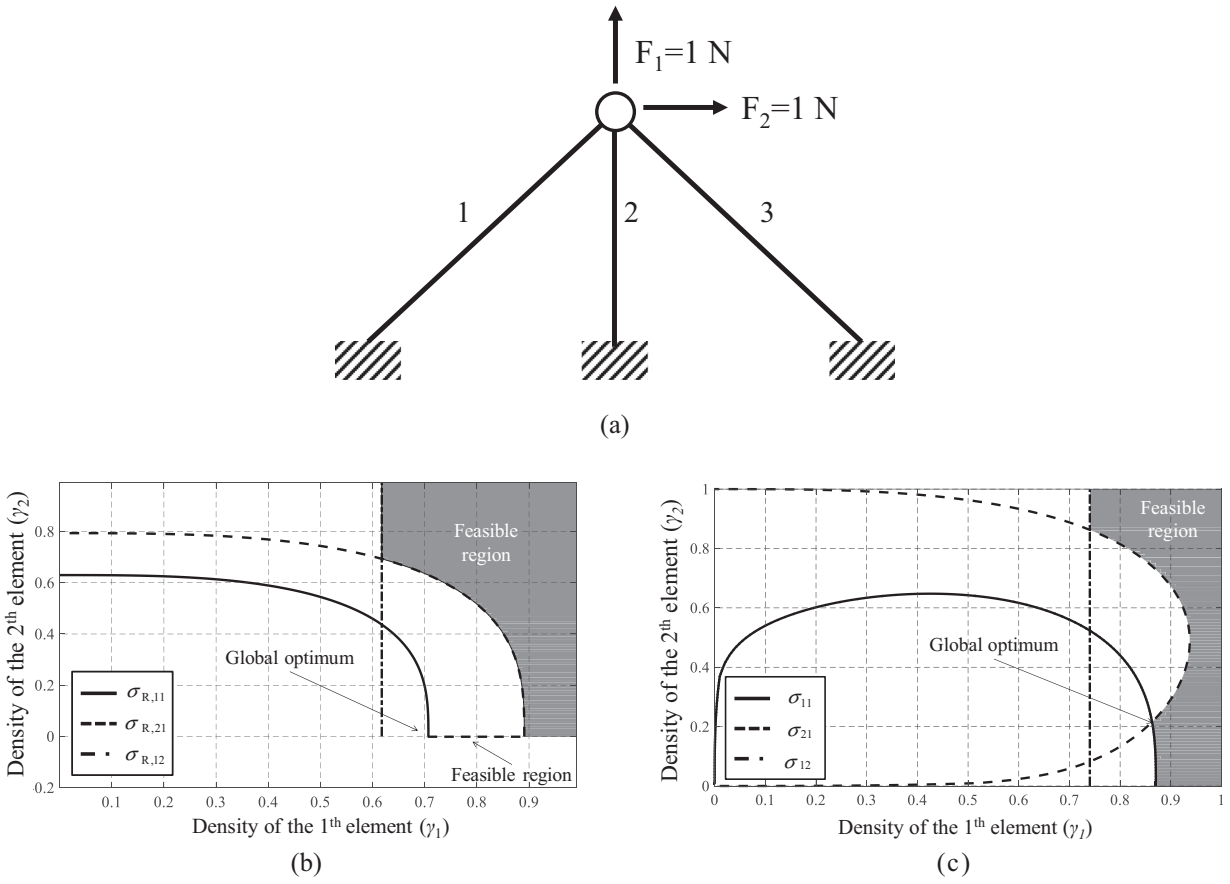

Fig. 6. A benchmark numerical example: (a) the three bar trusses structure problem, (b) feasible resign of the trusses example with n_s = 3 and (c) feasible resign of the trusses example with n_s = 0.5 (The benchmark problem is explaining the singularity issue in TO (see [12] and references therein). Note that the upper bound of the stress is also penalized ($\sigma_{ej} \leqslant \gamma_e^{n_s}\sigma_e^U$)).

method is employed for the equations of (8) ($n = 3$ and $n_s = 0.5$) that have been used for most STOM researches [21,24,26]. Then the stress values in (8) are plotted with respect to the various density values in Fig. 4.

Fig. 4 with 0.5 for n_s shows that the stress values of the two structures become identical (0.5 N/m^2) for $\gamma_R = 1$. And the stress value of the reinforcement structure become zero for $\gamma_R = 0$. Although the stress curve in Fig. 4(b) is not monotonically increased or decreased, it can interpolate the stress values for void and solid of the reinforcement. On the contrary, Fig. 5 shows the stress curves of the two layers with 3 for n_s.

Fig. 5(b) shows the stress behavior of the reinforcement with 3 for n_s. Compared to the stress values with 0.5 for n_s, first of all the stress behaviors, σ_R, are different, i.e., from concave to convex. With void for the reinforcement layer, the stress value of the reinforcement structure is approaching to zero and it becomes equal to the stress of the basic structure with the solid reinforcement layer. This simple study shows that both 0.5 and 3 (for n_s) values can be used to interpolate the stress value of the reinforcement.

2.3. Singularity issue example: three bar trusses example

For the sake of the numerical illustration of the singularity issue in TO, the optimization problem in (9) for the three bar trusses also can be considered; minimizing volume subject to stress constraints.

$$\begin{aligned} &\text{Min} \quad \sum_{e=1}^{NE} \gamma_e A_e L_e \\ &\text{S.t.} \quad \mathbf{K}(\gamma)\mathbf{U}_j = \mathbf{F}_j, \quad j = 1,2,\ldots,m, \\ &\quad \sigma_{ej} \leqslant \gamma_e^{n_s} \sigma_e^U, \quad j = 1,2,\ldots,m, \\ &\quad 0 \leqslant \gamma_e \leqslant 1 \end{aligned} \tag{9}$$

where the density of the e-th element, the area of the e-th element and the length of the e-th element are denoted by γ_e, A_e, L_e, respectively. The global stiffness matrix, displacement vector under the j-th load case and the j-th load case are represented as $\mathbf{K}$, $\mathbf{U}_j$ and $\mathbf{F}_j$, respectively (The number of load case is denoted as m). The e-th stress under the j-th load case, upper stress limit and penalty value are denoted as σ_{ej}, σ^U and p, respectively. In spite of the simplicity of the problem, this problem is known to be very difficult in terms of optimization because the large feasible domain is linked with the line to the global optimum as shown in Fig. 6(b).

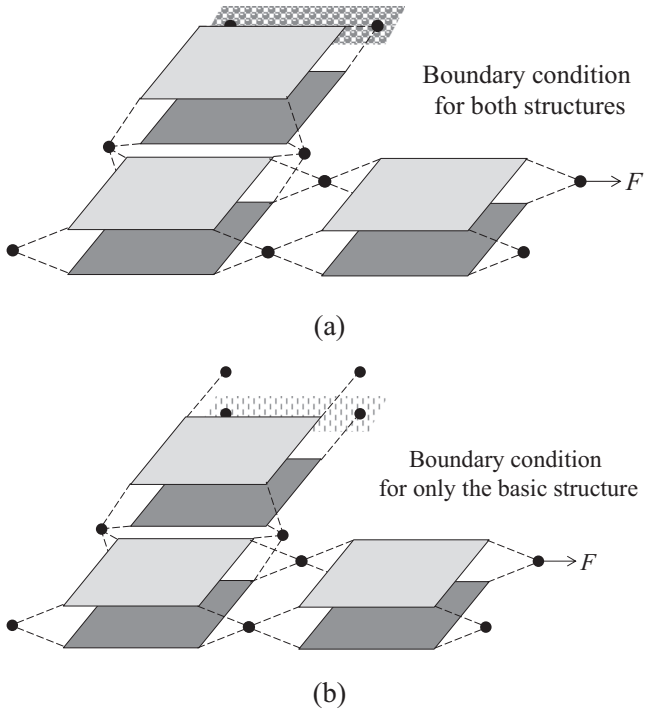

Fig. 8. Patch stacking method for the reinforcement and the basic structure: (a) boundary condition for both structures: the reinforcement and the basic structure and (b) boundary condition for only the basic structure.

In case of the reinforcement design, the stiffness matrix may be reformulated as follows:

$$\mathbf{k}_{\mathrm{B},e} = \frac{A_e E_{0,e}}{L_e}\begin{bmatrix} 1 & -1 \\ -1 & 1 \end{bmatrix}, \quad \mathbf{k}_{\mathrm{R},e} = \frac{A_e \gamma_e^n E_{0,e}}{L_e}\begin{bmatrix} 1 & -1 \\ -1 & 1 \end{bmatrix} \tag{10}$$

For the sake of simplicity, the following values are employed.

$$L_1 = L_3 = \sqrt{2}, \quad L_2 = 1, \quad A_e = 1, \quad E_{0,e} = 1, \quad \sigma_e^U = 0.4, \quad n = 3 \tag{11}$$

The displacement and the stress are computed as follows:

$$\mathbf{U}_1 = \begin{Bmatrix} 0 \\ \frac{1}{\frac{\gamma_1^{n}+1}{\sqrt{2}}+\gamma_2^n+1} \end{Bmatrix}, \quad \mathbf{U}_2 = \begin{Bmatrix} \frac{\sqrt{2}}{\gamma_1^n+1} \\ 0 \end{Bmatrix} \tag{12}$$

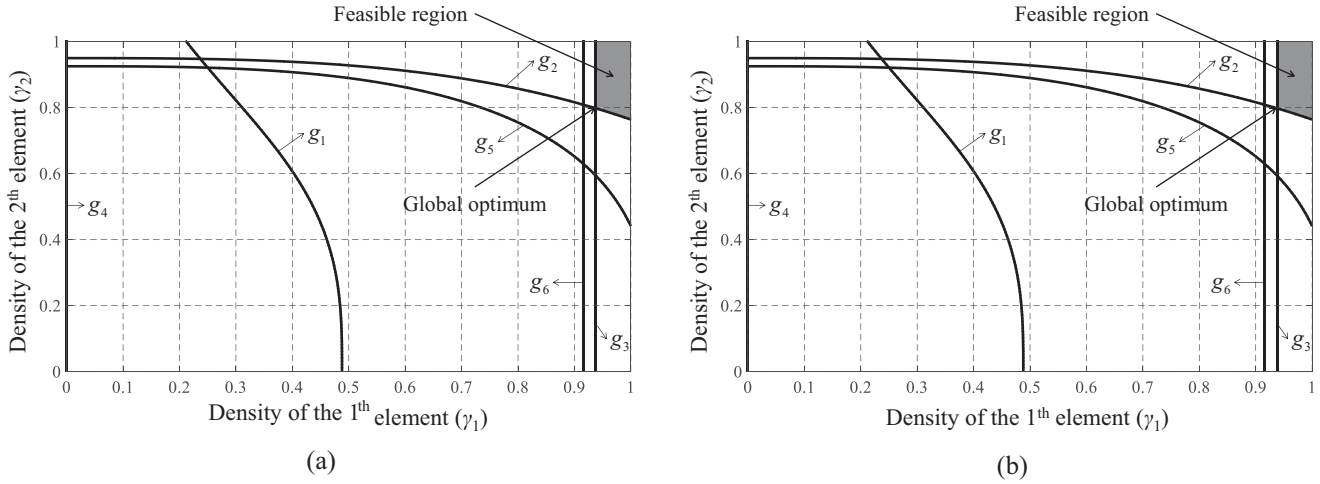

Fig. 7. Feasible region for the numerical example: the reinforcement stress constraint: (a) with $n_s = 3$ and (b) with $n_s = 0.5$.

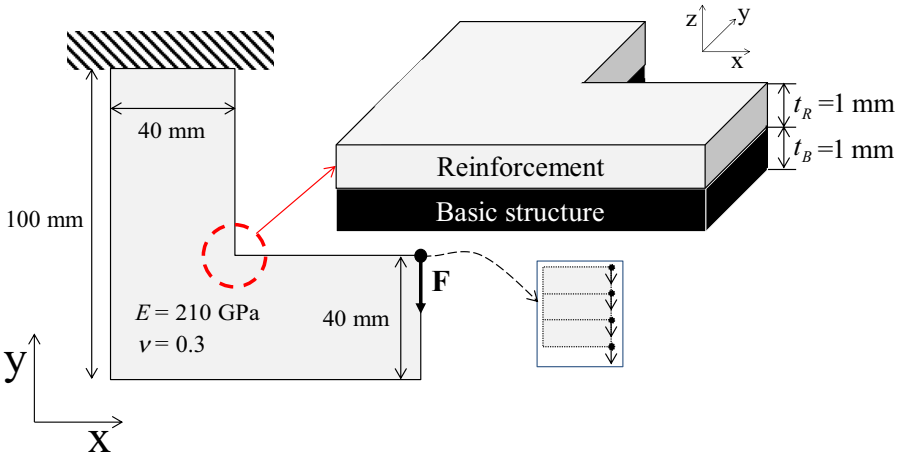

(a)

	Stress distribution of the reinforcement	Stress distribution of the basic structure
Reinforcement fill with solid (Density = 1)	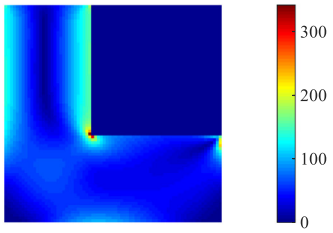 Maximum von-Mises stress: 341.858 MPa	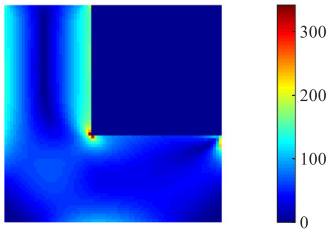 Maximum von-Mises stress: 341.858 MPa

(b)

	Stress distribution of the reinforcement	Stress distribution of the basic structure
Reinforcement fill with void (Density = 0)	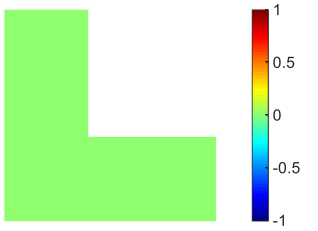 Maximum von-Mises stress: 0 MPa	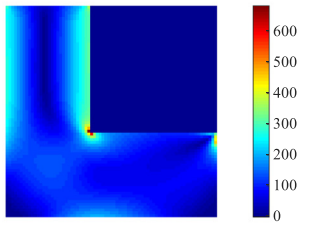 Maximum von-Mises stress: 683.715 MPa

(c)

Fig. 9. L-shaped bracket problem (The total number of elements in the design domain: 3600, **F**: 1000 MN (the number of applied node: 4), maximum allowable stress: 358 MPa, Young's modulus: 210 GPa, Poisson's ratio: 0.3): (a) design domain and geometric and boundary conditions, (b) stress distributions of the reinforcement and the basic structure with solid domain of the reinforcement and (c) stress distributions of the reinforcement and the basic structure with void reinforcement domain.

$$\sigma_{B,11} = \varepsilon_{11}E_{0,1} = \frac{1}{2A}, \quad \sigma_{B,21} = \varepsilon_{21}E_{0,2} = \frac{1}{A}, \quad \sigma_{B,12} = \varepsilon_{12}E_{0,1} = \frac{1}{\sqrt{2}B}, \quad A = \frac{\gamma_1^n + 1}{\sqrt{2}} + \gamma_2^n + 1, \quad B = (\gamma_1^n + 1) \tag{13.1}$$

$$\sigma_{B,22} = 0, \ \sigma_{B,31} = \sigma_{B,11}, \quad \sigma_{B,32} = -\sigma_{B,12} \tag{13.2}$$

$$\sigma_{R,11} = \varepsilon_1\gamma_1^{n_s}E_{0,1} = \frac{\gamma_1^{n_s}}{2A}, \quad \sigma_{R,21} = \varepsilon_{21}\gamma_2^{n_s}E_{0,2} = \frac{\gamma_2^{n_s}}{A}, \quad \sigma_{R,12} = \varepsilon_{12}\gamma_1^{n_s}E_{0,1} = \frac{\gamma_1^{n_s}}{\sqrt{2}B} \tag{14.1}$$

$$\sigma_{R,22} = 0, \quad \sigma_{R,31} = \sigma_{R,11}, \quad \sigma_{R,32} = -\sigma_{R,12} \tag{14.2}$$

Note that the stress value, $\sigma_{R,ej}$ and $\sigma_{B,ej}$, are the stress values of the e-th element for the j-th load case. With all the values, the following optimization minimizing volume subject to stress constraints can be formulated. Note that the stress values of the basic trusses and the reinforcement trusses are constrained simultaneously.

$$\begin{aligned} &\text{Min} \quad 2\sqrt{2}\gamma_1 + \gamma_2 \\ &\text{S.t.} \quad g_i \leqslant 0, i = 1, 2, \ldots, 6 \end{aligned} \tag{15.1}$$

$$\begin{aligned} &g_1 = \sigma_{B,11} - 0.4\gamma_1^{n_s}, \quad g_2 = \sigma_{B,21} - 0.4\gamma_2^{n_s}, \quad g_3 = \sigma_{B,12} - 0.4\gamma_1^{n_s}, \\ &g_4 = \sigma_{R,11} - 0.4\gamma_1^{n_s}, \quad g_5 = \sigma_{R,21} - 0.4\gamma_2^{n_s}, \quad g_6 = \sigma_{R,12} - 0.4\gamma_1^{n_s} \end{aligned} \tag{15.2}$$

With the same value for n and n_s without basic structure, it is known that the singularity issue becomes serious for TO since it is difficult to get global optimum with same penalty value for n and n_s (see [12] and references therein). For the reinforcement structure design, however, it is not problematic. Fig. 7 shows the stress curves with respect to the two design variables with 3 and 0.5 for n_s. Unlike the singular problem in Fig. 6, simply there is no singular point in the feasible domain regardless of the penalization value. All global points can be reached by the KKT condition; note that a gradient based optimizer can find out either the global optimum or the local optimum in Fig. 6.

3. Topology optimization formulation and sensitivity analysis

3.1. Topology optimization formulation

The following formulation is considered to conduct the continuum STOM for reinforcement. The objective function is the mass usage for reinforcement and the constraints are the maximum von-Mises stress constraints as follows:

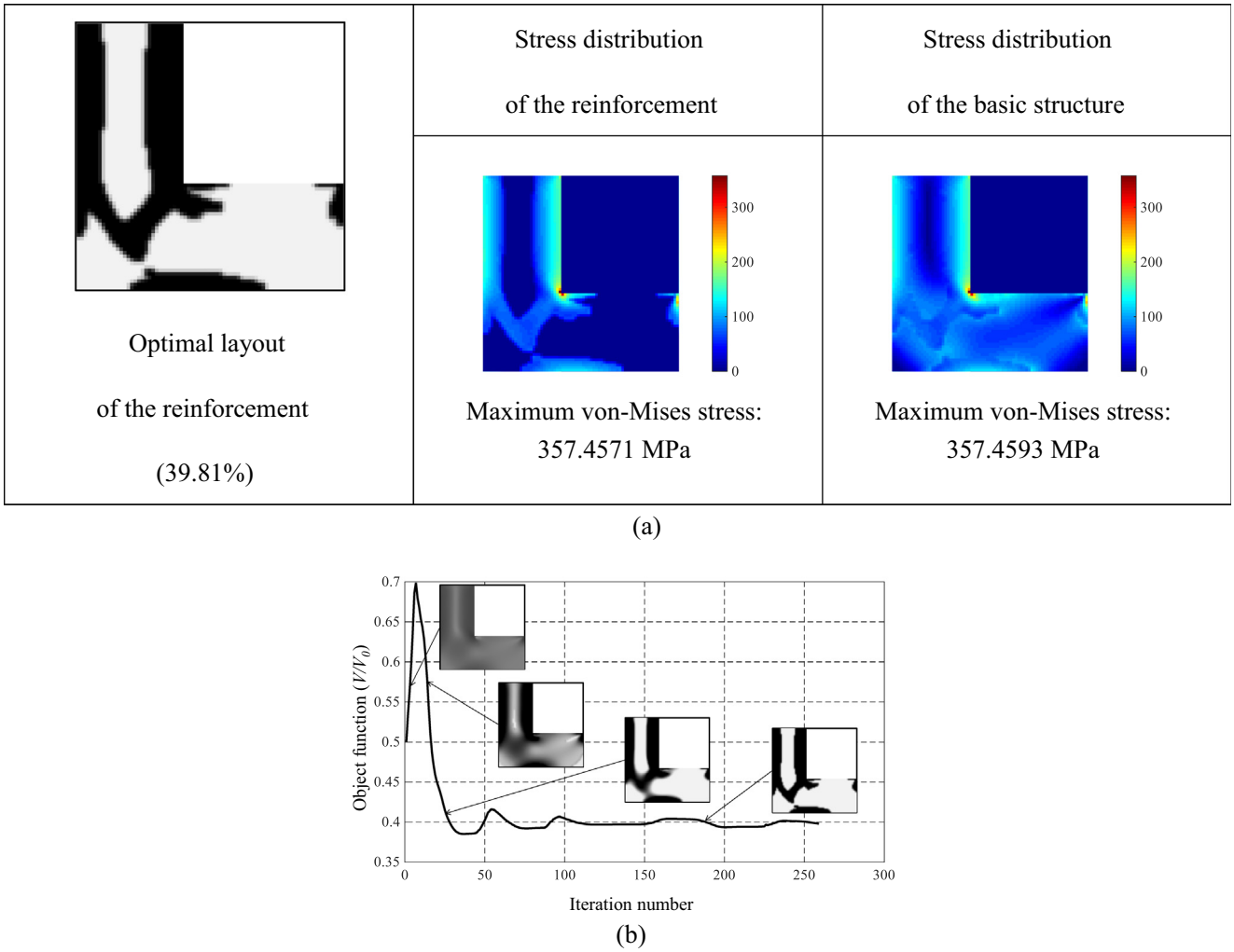

Fig. 10. Optimal reinforcement layout (Max allowable stress: 358 MPa, the volume of the optimal layout: 39.81% of the total reinforcement volume and the penalty values for the stiffness and the stress: $n = 3$, $n_s = 0.5$): (a) an optimal design and stress distribution of the basic structure and the reinforcement and (b) the optimization history.

$$\begin{aligned} &\underset{\tilde{\boldsymbol{\gamma}}}{\text{Minimize}} \quad V(\tilde{\boldsymbol{\gamma}}) = \sum_{e=1}^{NE} \tilde{\gamma}_e v_e (\tilde{\boldsymbol{\gamma}} : \text{filtered density}) \\ &\text{Subject to} \quad S_{\max} \leqslant S^* \\ &\text{where } S_{\max} = \max(S_e), e = 1, \ldots, NE \\ &\tilde{\boldsymbol{\gamma}} = \Xi(\boldsymbol{\gamma}) \text{ with the density filter } \Xi \end{aligned} \tag{16}$$

where the total volume, the e-th element volume, the von-Mises stress of the e-th element and maximum allowable stress are denoted by V, v_e, S_e and S^*, respectively. The NE design variables are $\boldsymbol{\gamma}$. As the maximum operator in the above formulation is non-differentiable, the P-norm approach is considered with the correction factor.

$$S_{\max} \equiv C^{iter} \langle S_{PN} \rangle = C^{iter} \left(\sum_{e=1}^{NE} S_e^p \tilde{\gamma}_e \right)^{\frac{1}{p}} \tag{17}$$

$$C^{iter} = \alpha \frac{S_{\max}^{iter-1}}{\langle S_{PN} \rangle^{iter-1}} + (1-\alpha) C^{iter-1} \quad 0 < \alpha < 1 \tag{18}$$

where C^{iter}, $S_{\max}^{iter}$, p and α are the correction factor at the $iter$-th optimization iteration, the real maximum value of von-Mises stress at the $iter$-th optimization iteration, the p value and the damping factor, respectively. The p value used for p-norm approximation is set to 3 and the value of α is set to 0.5 in this research.

3.2. Sensitivity analysis

It is essential to derive the sensitivity value of the von-Mises stress. With the adjoint variable, λ, the following sensitivity analysis can be formulated.

$$\frac{d\langle S_{PN} \rangle}{d\tilde{\gamma}_e} = \frac{\partial \langle S_{PN} \rangle}{\partial \tilde{\gamma}_e} + \frac{\partial \langle S_{PN} \rangle}{\partial S_e} \frac{\partial S_e}{\partial \boldsymbol{\sigma}_e} \frac{\partial \boldsymbol{\sigma}_e}{\partial \tilde{\gamma}_e} + \sum_{e^*=1}^{2NE} \frac{\partial \langle S_{PN} \rangle}{\partial S_{e^*}} \frac{\partial S_{e^*}}{\partial \boldsymbol{\sigma}_{e^*}} \frac{\partial \boldsymbol{\sigma}_{e^*}}{\partial \mathbf{U}} \frac{d\mathbf{U}}{d\tilde{\gamma}_e} \tag{19}$$

The Lagrange multiplier is computed by the following:

$$\mathbf{K}^{\mathrm{T}} \boldsymbol{\lambda} = -\sum_{e^*=1}^{2NE} \frac{\partial \langle S_{PN} \rangle}{\partial S_{e^*}} \left(\frac{\partial S_{e^*}}{\partial \boldsymbol{\sigma}_{e^*}} \frac{\partial \boldsymbol{\sigma}_{e^*}}{\partial \mathbf{U}} \right)^{\mathrm{T}} \tag{20}$$

The final sensitivity values of the p-norm stress can thus be obtained.

$$\frac{d\langle S_{PN} \rangle}{d\tilde{\gamma}_e} = \frac{\partial \langle S_{PN} \rangle}{\partial \tilde{\gamma}_e} + \frac{\partial \langle S_{PN} \rangle}{\partial S_e} \frac{\partial S_e}{\partial \boldsymbol{\sigma}_e} \frac{\partial \boldsymbol{\sigma}_e}{\partial \tilde{\gamma}_e} + \boldsymbol{\lambda}^{\mathrm{T}} \frac{d\mathbf{K}}{d\tilde{\gamma}_e} \mathbf{U} \tag{21}$$

3.3. Multi-material and material dependent boundary condition

It was noticed that it is possible to use different material for reinforcement and sometimes it is also desirable to compose material dependent boundary condition [45–47]. To consider them, the patch stacking method in Fig. 8 which is our previous contribution

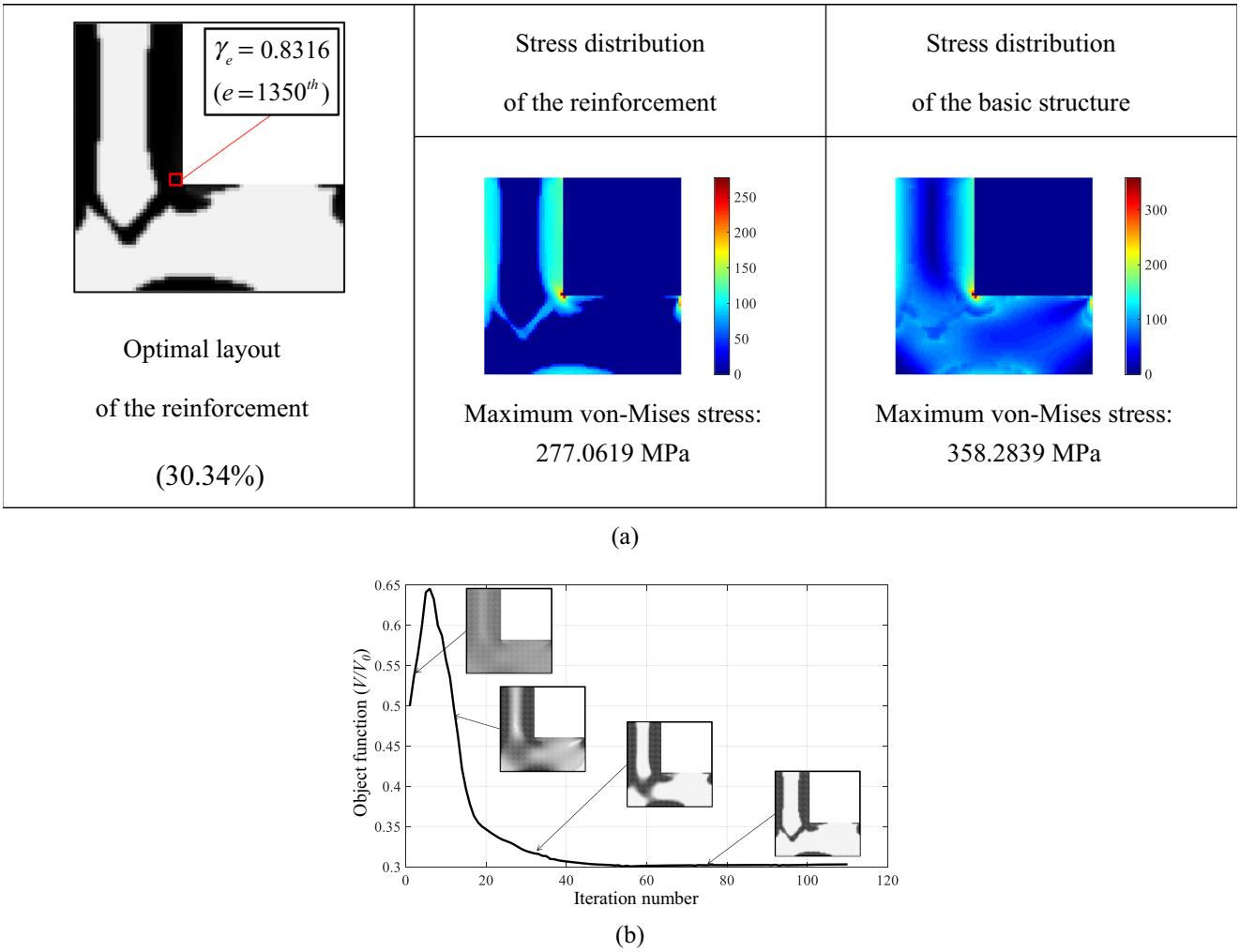

Fig. 11. An optimal reinforcement layout (Max allowable stress: 358 MPa, the volume of the optimal layout: 30.34% of the total reinforcement volume and the penalty values for the stiffness and the stress: $n = 3$, $n_s = 3$): (a) an optimal layout and stress distribution of the basic structure and the reinforcement and (b) the optimization history.

[45–47], is implemented here. The ideas of the patch stacking method are that the FE elements for reinforcement are juxtaposed to the FE elements for the basic structure and the material boundary conditions are also applicable as shown in Fig. 8(a).

4. Numerical examples

To show the validity of the developed approach, this chapter solves several benchmark STOM problems. For the optimization algorithm, the method of moving asymptotes is employed [48].

4.1. Example 1: L-bracket problem

For the first numerical example, we consider the L-shape bracket problem in Fig. 9 whose optimal layouts have been presented by other relevant researches [21,24,26,30,31]. One of the differences compared with the other researches is the juxtaposing the reinforcement layer on the basic structure in Fig. 9 and the optimization procedure finds out a reinforcement structure attached to the basic structure to constrain the stress values. The specific configurations of the design domain and the boundary conditions are illustrated in Fig. 9(a).

In Fig. 9(a), the upper part with the gray color and the bottom structure with black color represent the reinforcement structure and the basic structure, respectively. Note that only the reinforcement domain is set to a design domain. In the standard STOM problem for void or solid design, a design with the rounded corner at the reentrance corner should be obtained (see [21,24,26,30,31] and references therein). With the present reinforcement design formulation, it is expected that some optimal reinforcement designs can be obtained. Before optimization, the von-Mises stress distributions of solid and void design are plotted in Fig. 9(b) and (c). With those results, the maximum allowable stress is set to 358 MPa for the optimization.

Fig. 10 shows the optimal design considering the stress distributions of the reinforcement with the *qp*-relaxation method ($n = 3$, $n_s = 0.5$) and the basic structure. Both the stress values of the reinforcement structure and the basic structure are equal for solid reinforcement structure. Otherwise, the stresses of the basic structure are larger than the stresses of the reinforcement in the design domain. The stress concentration phenomena are well modeled at the reentrance corner and the optimization algorithm does gather more material at the reentrance corner; because of the basic structure, a rounded reinforcement design is not anymore preferred.

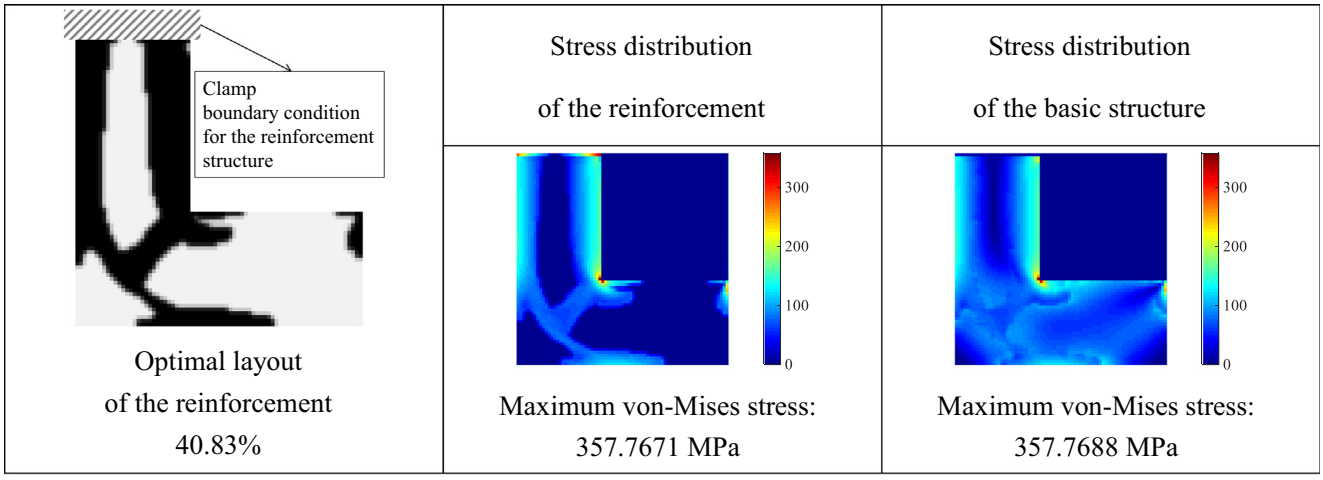

Fig. 12. Optimal layouts with material dependent boundary conditions (Max allowable stress: 358 MPa, the penalty values for the stiffness and the stress: $n = 3$, $n_s = 0.5$): (a) with clamp boundary condition for the reinforcement structure and (b) the clamp boundary condition for the basic structure.

In Fig. 11, we also test the same penalization values with the stiffness, i.e., $n = 3$, $n_s = 3$ to check the singularity issue for the reinforcement design. The volume ratio of the reinforcement is 30.34% of the total reinforcement volume. The overall optimal shapes in Fig. 10 and Fig. 11 are almost similar and the design in Fig. 10 uses more mass due to the different stress interpolation ($n = 3$, $n_s = 0.5$). In the intermediate density, the maximum stress with 0.5 for n_s is higher than the maximum stress with 3 for n_s. So, the more mass is used to reduce the stress level. Although there is a slight difference in the amount of material used, the singularity issue is not serious in the reinforcement design since we can get similar optimal results with 0.5 or 3 for n_s.

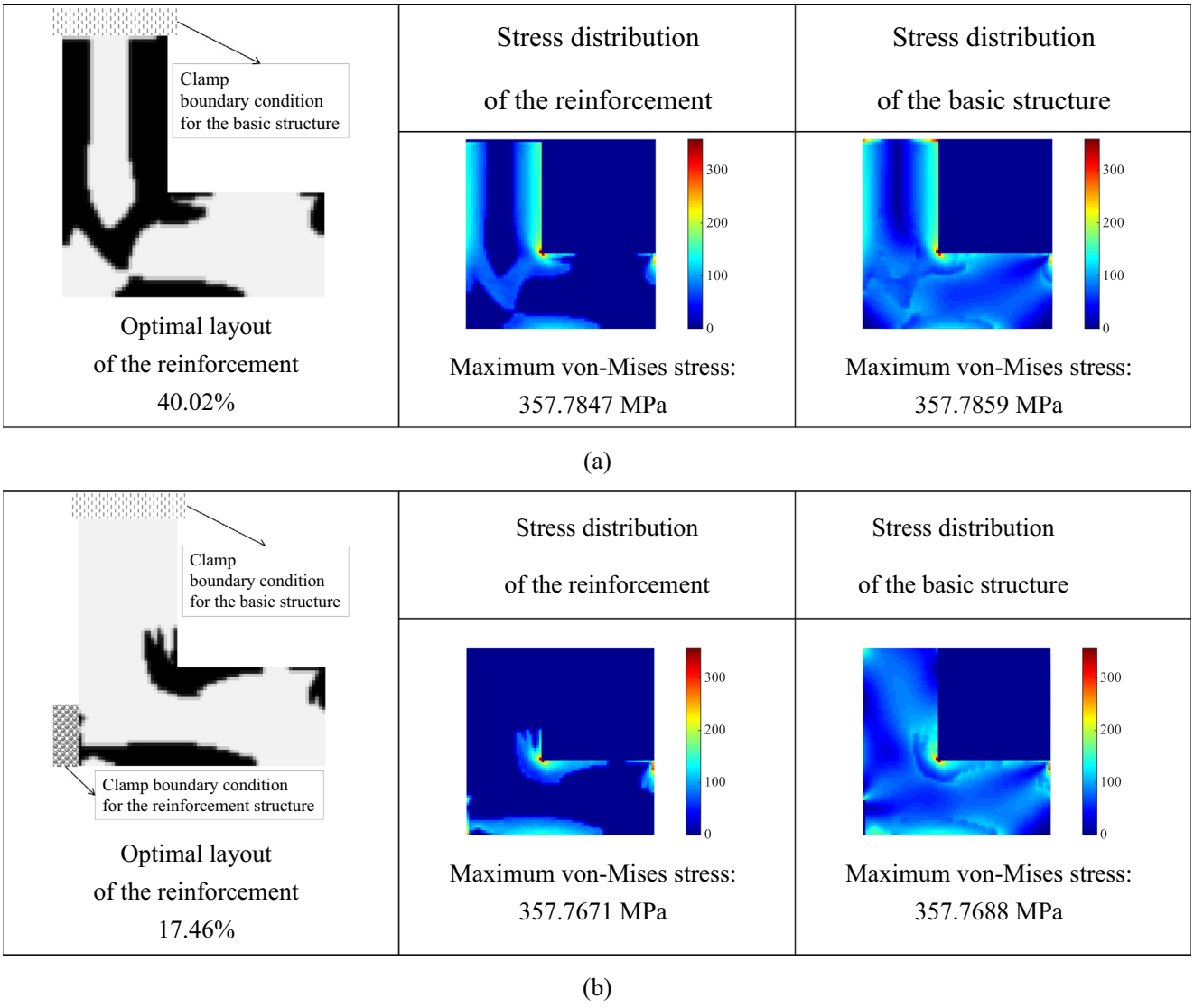

Fig. 13. Optimal layouts with material dependent boundary conditions (Max allowable stress: 358 MPa, the penalty values for the stiffness and the stress: $n = 3$, $n_s = 0.5$): (a) with clamp boundary condition for the basic structure and (b) additional boundary condition for the reinforcement structure.

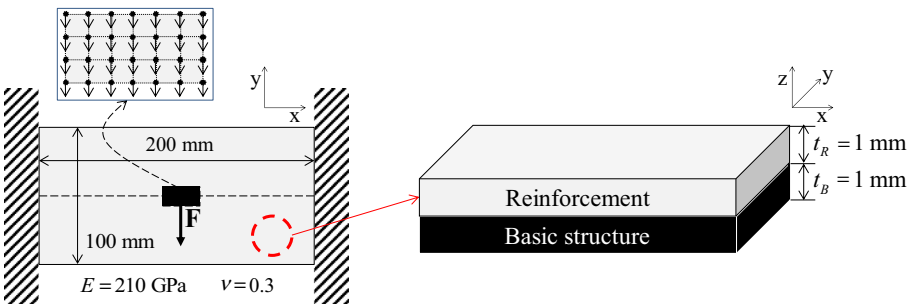

Fig. 14. The bridge structure problem (The total number of elements in the design domain: 2178, **F**: 20,000 MN, maximum allowable stress: 300 MPa, Young's modulus: 210 GPa, Poisson's ratio: 0.3).

4.1.1. Multiple materials and material-dependent boundary condition

For further study, multiple material and material-dependent boundary conditions are considered. Fig. 12(a) and (b) show the optimal layouts with the clamp boundary conditions only for (a) the reinforcement structure and (b) the basic structure. There are small different because the same material is used for the reinforcement structure and the basic structure. But a closer investigation of the designs along the boundary reveals that there is no reinforcement structure at Fig. 12(b).

To investigate the effects of material dependent boundary condition, Fig. 13 shows the optimal layouts with the different boundary conditions. Due to the different locations of the clamp boundary conditions, the significant differences in optimal layout can be obtained.

4.2. Example 2: Bridge problem

For the second example, the bridge problem is considered in Fig. 14. The both sides of the design domain are clamped and a distributed downward load with 715 MN is applied at the each node (the number of applied nodes of the load is 28).

As in the first example, there is the basic structure and the present STOM algorithm should design the reinforcement structure. Figs. 15 and 16 show the reinforcement designs with $n = 3$, $n_s = 0.5$ and with $n = 3$, $n_s = 3$, respectively.

Unlike the first example, the two designs have some differences. First of all, the design in Fig. 15 doesn't have the four arms connecting the center structure to the four corner edges but the design of Fig. 16 has the connecting arms. However the two designs have some similarities including the three internal holes and the bar structures at the bottom and the upper part.

4.2.1. Effects of the maximum allowable stress

To see the effect of the maximum allowable stress in the STOM, Fig. 17 shows the three different optimal layouts with three different maximum allowable stress values, i.e., 260 MPa, 280 MPa and 320 MPa. As expected, with a low maximum allowable stress, a thicker reinforcement design is obtained where lighter designs are obtained with lager maximum allowable stress values.

4.2.2. Multiple materials and material-dependent boundary condition

The results with the patch stacking method for the second present example are shown below. In the first case, the left side of the reinforcement and the right side of the basic structure are clamped. And the second case, the left side of the basic structure and the right side of the reinforcement are clamped. The results are optimized according to the boundary conditions (see Fig. 18)

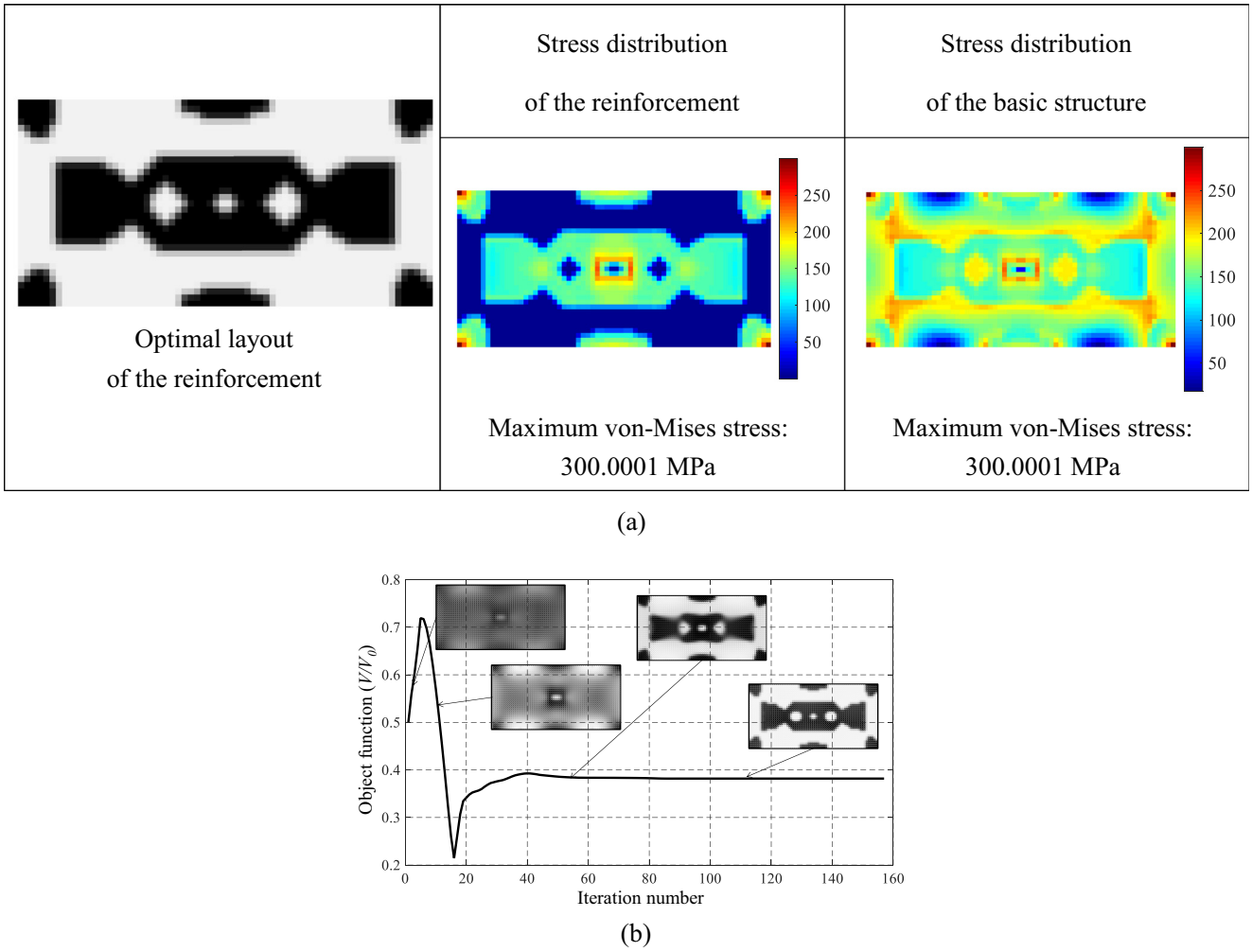

Fig. 15. Optimal reinforcement layouts (Max allowable stress: 358 MPa, the volume of the optimal layout: 37.63% of the total reinforcement volume, the penalty values for the stiffness and the stress: $n = 3$, $n_s = 0.5$: (a) optimal layout and stress distribution of the basic structure and the reinforcement and (b) the optimization history.

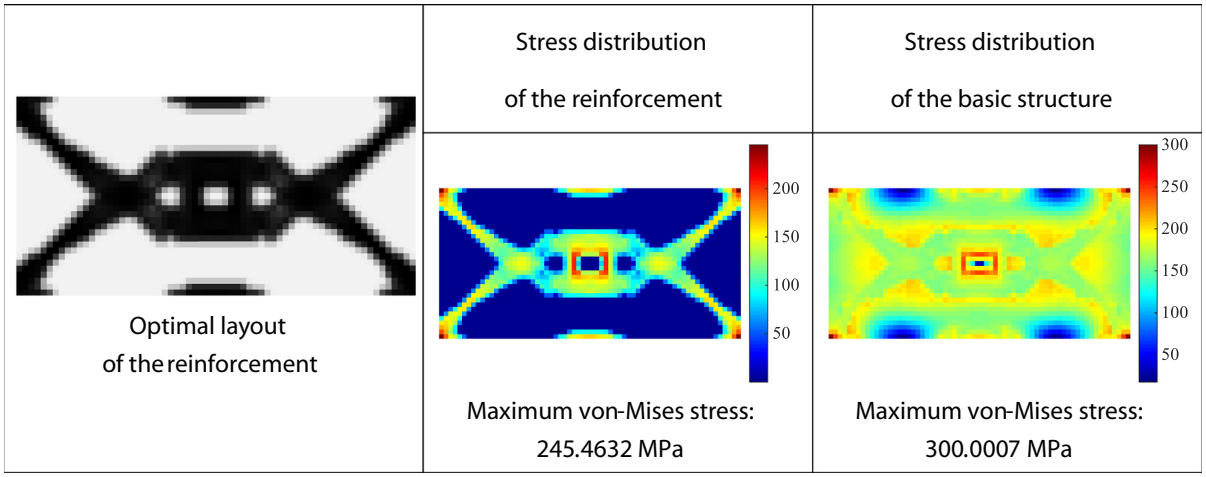

Fig. 16. Optimal reinforcement layouts Optimal reinforcement layouts (Max allowable stress: 358 MPa, the volume of the optimal layout: 33.71% of the total reinforcement volume, the penalty values for the stiffness and the stress: $n = 3$, $n_s = 3$): (a) an optimal layout and stress distribution of the basic structure and the reinforcement and (b) the optimization history.

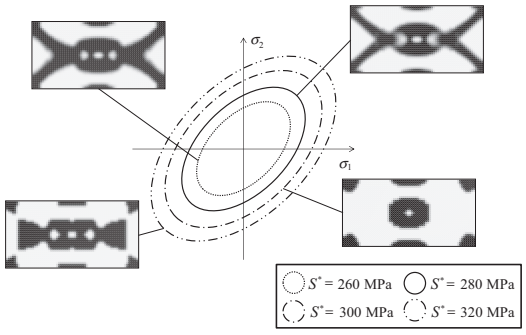

(a)

$S^* = 260$ MPa	$S^* = 280$ MPa	$S^* = 300$ MPa	$S^* = 320$ MPa
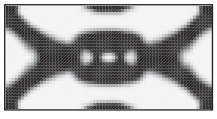	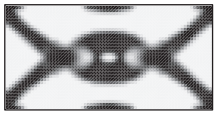	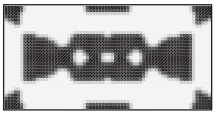	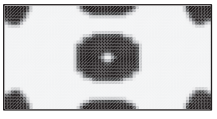
45.74 % of the total reinforcement volume	39.04 % of the total reinforcement volume	37.63 % of the total reinforcement volume	23.08 % of the total reinforcement volume

(b)

Fig. 17. Effect of the maximum allowable stress as constraint: (a) the difference of the optimal result with respect to maximum allowable stress and (b) the difference of converged volume.

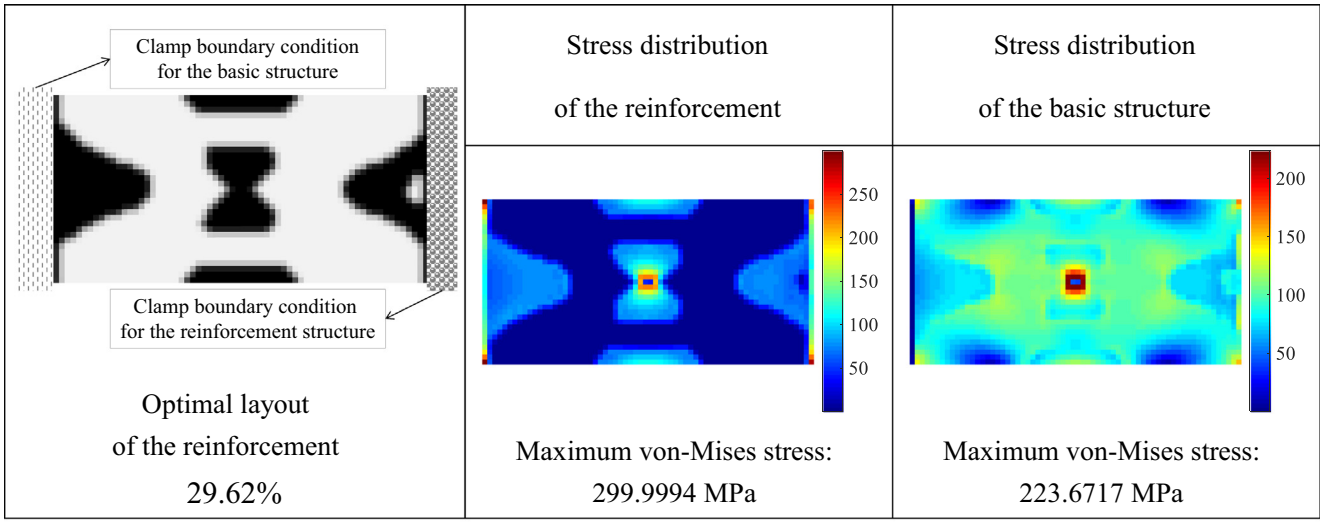

(a)

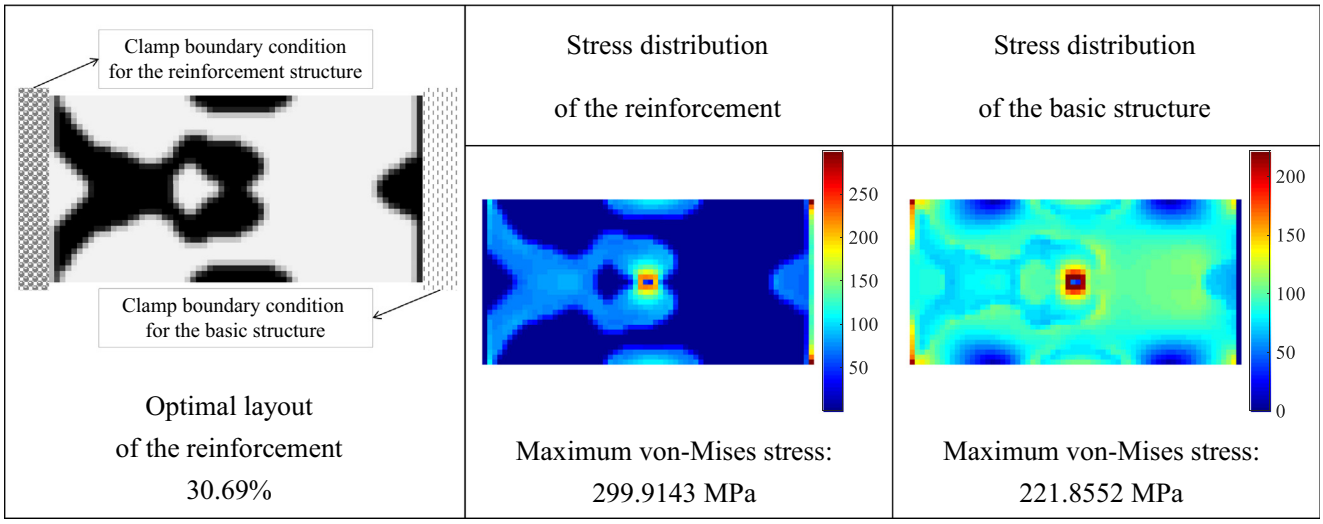

(b)

Fig. 18. Optimal layouts with material dependent boundary conditions (Max allowable stress: 300 MPa, the penalty values for the stiffness and the stress: $n = 3$, $n_s = 0.5$): (a) for the first boundary condition and (b) the second boundary condition.

5. Conclusions

The present research studies the stress discrepancy issue and the stress interpolation function for the optimal reinforcement layer design under in-plane load. With the existing *qp*-relaxation method using the different penalization factors for the forward analysis and the stress analysis, it is found that another type of stress discrepancy between the stress values of the reinforcement by different n_s values exist. In other words, with 0.5 for n_s, the stress curve is convex but with 3 for n_s it is changed to concave. This discrepancy can lead different optimal layouts of reinforcement structure. In our numerical examples, more materials are needed to design the reinforcement with the convex stress curve with 0.5 for n_s than with the concave stress curve with 3 for n_s. To illustrate this issue and obtain physically reasonable reinforcement design, the present research studies the stress behaviors of a simple structure consisting with two elastic springs that represent basic structure and reinforcement structure. We can conclude that the singularity issue is not serious for the STOM for reinforcement structure design and similar optimal results can be obtained with 0.5 or 3 for n_s. The stress constraints with zeros for the design variables are not considered in optimization algorithm by multiplying the design variables to the *p*-norm of the stress values of reinforcement design. By increasing or decreasing the maximum allowable stress values, thinner and thicker optimal reinforcement structures can be obtained. For future research topics, the study should be extended for plate, curved shell or multilayered composite structures.

Acknowledgements

This work was supported by the National Research Foundation of Korea (NRF) grant funded by the Korea government (MEST) (NRF-2015R1A2A2A11027580).

References

[1] Bendsoe MP, Sigmund O. Topology optimization: theory, methods and applications. Springer Science & Business Media; 2003.
[2] Bendsøe MP, Sigmund O. Material interpolation schemes in topology optimization. Arch Appl Mech 1999;69:635–54.

[3] Bruggi M, Venini P. Eigenvalue-based optimization of incompressible media using mixed finite elements with application to isolation devices. Comput Method Appl M 2008;197:1262–79.
[4] Moon SJ, Yoon GH. A newly developed qp-relaxation method for element connectivity parameterization to achieve stress-based topology optimization for geometrically nonlinear structures. Comput Method Appl M 2013;265:226–41.
[5] Sigmund O. On the design of compliant mechanisms using topology optimization*. J Struct Mech 1997;25:493–524.
[6] Sigmund O. A 99 line topology optimization code written in Matlab. Struct Multidiscip O 2001;21:120–7.
[7] Suzuki K, Kikuchi N. A homogenization method for shape and topology optimization. Comput Method Appl M 1991;93:291–318.
[8] Takezawa A, Kitamura M. Phase field method to optimize dielectric devices for electromagnetic wave propagation. J Comput Phys 2014;257:216–40.
[9] Takezawa A, Yoon GH, Jeong SH, Kobashi M, Kitamura M. Structural topology optimization with strength and heat conduction constraints. Comput Method Appl M 2014;276:341–61.
[10] Wang Y, Luo Z, Kang Z, Zhang N. A multi-material level set-based topology and shape optimization method. Comput Method Appl M 2015;283:1570–86.
[11] Allaire G, Jouve F, Maillot H. Topology optimization for minimum stress design with the homogenization method. Struct Multidiscip O 2004;28:87–98.
[12] Bruggi M. On an alternative approach to stress constraints relaxation in topology optimization. Struct Multidiscip O 2008;36:125–41.
[13] Bruggi M, Duysinx P. Topology optimization for minimum weight with compliance and stress constraints. Struct Multidiscip O 2012;46:369–84.
[14] Bruggi M, Venini P. A mixed FEM approach to stress-constrained topology optimization. Int J Numer Meth Eng 2008;73:1693–714.
[15] Burger M, Stainko R. Phase-field relaxation of topology optimization with local stress constraints. SIAM J Control Optim 2006;45:1447–66.
[16] Cheng G, Jiang Z. Study on topology optimization with stress constraints. Eng Optim 1992;20:129–48.
[17] Duysinx P, Bendsoe MP. Topology optimization of continuum structures with local stress constraints. Int J Numer Meth Eng 1998;43:1453–78.
[18] Guo X, Zhang W, Zhong W. Stress-related topology optimization of continuum structures involving multi-phase materials. Comput Method Appl M 2014;268:632–55.
[19] Guo X, Zhang WS, Wang MY, Wei P. Stress-related topology optimization via level set approach. Comput Method Appl M 2011;200:3439–52.
[20] Holmberg E, Torstenfelt B, Klarbring A. Global and clustered approaches for stress constrained topology optimization and deactivation of design variables. In: 10th World congress on structural and multidisciplinary optimization, May 19–24, 2013, Orlando, Florida, USA. p. 1–10.
[21] Jeong SH, Park SH, Choi DH, Yoon GH. Topology optimization considering static failure theories for ductile and brittle materials. Comput Struct 2012;110:116–32.
[22] Jeong SH, Yoon GH, Takezawa A, Choi D-H. Development of a novel phase-field method for local stress-based shape and topology optimization. Comput Struct 2014;132:84–98.
[23] Kocvara M, Stingl M. Solving stress constrained problems in topology and material optimization. Struct Multidiscip O 2012;46:1–15.
[24] Le C, Norato J, Bruns T, Ha C, Tortorelli D. Stress-based topology optimization for continua. Struct Multidiscip O 2010;41:605–20.
[25] Lee E, James KA, Martins JRA. Stress-constrained topology optimization with design-dependent loading. Struct Multidiscip O 2012;46:647–61.
[26] Lee JW, Yoon GH, Jeong SH. Topology optimization considering fatigue life in the frequency domain. Comput Math Appl 2015;70:1852–77.
[27] Luo Y, Wang MY, Kang Z. An enhanced aggregation method for topology optimization with local stress constraints. Comput Method Appl M 2013;254:31–41.
[28] Luo YJ, Kang Z. Topology optimization of continuum structures with Drucker-Prager yield stress constraints. Comput Struct 2012;90–91:65–75.
[29] Paris J, Martinez S, Nogueira X, Colominas I, Navarrina F, Casteleiro M. A minimum weight formulation with stress constraints in topology optimization of structures. Rev Internacional de Metodos Numericos Para Calculo y Diseno en Ingenieria 2012;28:33–48.
[30] Paris J, Navarrina F, Colominas I, Casteleiro M. Topology optimization of continuum structures with local and global stress constraints. Struct Multidiscip O 2009;39:419–37.
[31] Paris J, Navarrina F, Colominas I, Casteleiro M. Block aggregation of stress constraints in topology optimization of structures. Adv Eng Softw 2010;41:433–41.
[32] París J, Navarrina F, Colominas I, Casteleiro M. Improvements in the treatment of stress constraints in structural topology optimization problems. J Comput Appl Math 2010;234:2231–8.
[33] París J, Navarrina F, Colominas I, Casteleiro M. Stress constraints sensitivity analysis in structural topology optimization. Comput Method Appl M 2010;199:2110–22.
[34] Qiu GY, Li XS. A note on the derivation of global stress constraints. Struct Multidiscip O 2010;40:625–8.
[35] Rozvany GIN. Difficulties in truss topology optimization with stress, local buckling and system stability constraints. Struct Optim 1996;11:213–7.
[36] Svanberg K, Werme M. Sequential integer programming methods for stress constrained topology optimization. Struct Multidiscip O 2007;34:277–99.
[37] Yang R, Chen C. Stress-based topology optimization. Struct. Optimization 1996;12:98–105.
[38] Paris J, Colominas I, Navarrina F, Casteleiro M. Parallel computing in topology optimization of structures with stress constraints. Comput Struct 2013;125:62–73.
[39] Luo Y, Zhou M, Wang MY, Deng Z. Reliability based topology optimization for continuum structures with local failure constraints. Comput Struct 2014;143:73–84.
[40] Goo S, Wang S, Hyun J, Jung J. Topology optimization of thin plate structures with bending stress constraints. Comput Struct 2016;175:134–43.
[41] Lee K, Ahn K, Yoo J. A novel P-norm correction method for lightweight topology optimization under maximum stress constraints. Comput Struct 2016;171:18–30.
[42] Amir O. A topology optimization procedure for reinforced concrete structures. Comput Struct 2013;114:46–58.
[43] Luo Y, Wang MY, Zhou M, Deng Z. Topology optimization of reinforced concrete structures considering control of shrinkage and strength failure. Comput Struct 2015;157:31–41.
[44] Logan DL. A first course in the finite element method: Cengage. Learning 2011.
[45] Jeong SH, Choi D-H, Yoon GH. Separable stress interpolation scheme for stress-based topology optimization with multiple homogenous materials. Finite Elem Anal Des 2014;82:16–31.
[46] Yoon GH. Topology optimization for nonlinear dynamic problem with multiple materials and material-dependent boundary condition. Finite Elem Anal Des 2011;47:753–63.
[47] Gao T, Xu P, Zhang W. Topology optimization of thermo-elastic structures with multiple materials under mass constraint. Comput Struct 2016;173:150–60.
[48] Svanberg K. The method of moving asymptotes - a new method for structural optimization. Int J Numer Meth Eng 1987;24:359–73.